 doi:10.20944/preprints202012.0574.v1

Article

Nonlinear problems of equilibrium charge state transport in hot plasmas

Vladimir A. Shurygin

National Research Centre "Kurchatov Institute", P.O. Box 3402, Ploschad akademika Kurchatova 1, Moscow, 123182, Russian Federation; Shurygin_VA@nrcki.ru

Abstract: The general coupling between particle transport and ionization-recombination processes in hot plasma is considered on the key concept of equilibrium charge state (CS) transport. A theoretical interpretation of particle and CS transport is gained in terms of a two-dimensional (2D) Markovian stochastic (random) processes, a discrete 2D Fokker-Plank-Kolmogorov equation (in charge and space variables) and generalized 2D coronal equilibrium between atomic processes and particle transport. The basic tool for analysis of CS equilibrium and transport is the equilibrium cell (EC) (two states on charge and two on space), which presents (i) a unit phase volume, (ii) the characteristic scale of local equilibrium, (iii) a comprehensive solution for the simplest nonlinear relations between transport and atomic processes. The approach opens up new perspectives on transport studies: (i) the direct modelling of equilibrium and transport of impurity using the atomic data base, (ii) recovery of the complete recombination rate profile based on knowledge of density profiles and ionization rate profiles, (iii) the local transport analysis, based on the reduction of the equilibrium set to the single EC (in particular, central or edge), (iv) analysis of the reduced transport coefficients (diffusion and convection) on the density profile measurements.

Keywords: magnetically confined plasma; impurity, charge state, transport, coronal equilibrium; diffusion coefficient

1. Introduction

Understanding the behavior and control of impurities as an inevitable component of magnetically confined plasmas continue to be a topic of considerable importance in fusion research programs. Steady state mode of operation with impurity equilibrium is of vital to the success in modern experimental studies of improved confinement and stability of standard H-modes on tokamaks and stellarators [1, 2].

In these devices, the radial transport of plasma particles across the magnetic field is accompanied by random change in their charge states (CS's) due to ionization-recombination processes. The probabilistic imposition of these atomic processes on the transport of impurity particles occurs in an unusual phase space, which includes the discrete space of (Z+1) CS's. So, the resulting generalized transport turns out to be at least two-dimensional (2D), while its structure involving an intersection of statistically independent processes is unexpectedly complicated. A consistent approach to this 2D transport problem could suggest the use of multidimensional (mD) Fokker-Planck-Kolmogorov equation [3-5].

Meanwhile, for more than 4 decades, the description of impurity transport remained implicitly simplified and was reduced to a 1D diffusive-convective model (DCM), represented in 1D impurity transport codes (see, for example, the STRAHL code [6]). Here, the standard 1D continuity equation was supplemented in the right-hand part with also a standard 1D flux balance of ionization-recombination processes interpreted as random sources and sinks of charged particles. So, the required 2D description was just replaced by sum of these 1D parts. The corresponding misinterpretation fell into a fatal contradiction with the systematic approach that the theory of the generalized FPKE could provide. Moreover, the formal discretization of the DCM equations

 doi:10.20944/preprints202012.0574.v1

revealed and returned this 2D transport problem but only in the form of a 2D grid model (GM) in charge and radial variables (see discussion in [6] on page 6).

In the practice of modeling medium and heavy impurities, that is, with an increase in the rates of ionization-recombination, it was found that the DCM sensitivity to the empirical transport coefficients remains extremely low [7-13] and just unacceptable for W impurity [14, 15].

Nevertheless, the leading role in interpreting the behavior of impurities was assigned to various mechanisms of particle transport in the 6D phase space (of coordinates and velocities) in terms of the Boltzmann kinetic equation and its consequences carefully studied in the neoclassical transport theory [16]. But in the basic equations of neoclassical transport, the charge state as a mandatory variable was ignored along with impurity charge state space (see, e.g., Equation (2.2) in [16]). The essential cross terms (mixed derivatives) representing the coupling of atomic processes with particle transport were also lost.

A new approach to this problem was based on the concept of impurity CS transport [17-21]. First of all, it was required to make a terminology distinction between particle and CS transports, which proved useful for clarifying the structure and probabilistic nature of transport. However, the main unresolved physical problem was that 1D (radial) transport of particles would have to be clearly distinguished from the generalized 2D transport in the proper 2D phase space, where the particle transport is only part of CS transport.

Indeed, although, there is no particle without CS, as well as no CS of no particle, but there is a fundamental difference between the transport of particles and the transport of their CS's due to ionization and recombination processes. In fact, let the probability of the transfer of CS's by particles be $H(P)$, and by atomic processes be $H(A)$, then the probability of events $P+A$ is expressed, as is known, by the general formula

$$H(P+A) = H(P) + H(A) - H(P) \cdot H(A), \quad (1)$$

which shows that the generalized transport includes three mandatory components: (i) CS transport by particles or *p*-transport, (ii) CS transport by atomic processes or *a*-transport, and, finally, (iii) CS transport represented by probabilistic intersection of *a*-transport and *p*-transport but irreducible to any of them. Note that the latter is the most represented case of events related to impurity transport in plasma and analyzed in Formula (1). However, it is also seen that DCM is limited to analyzing only the first two, implicitly (and erroneously) assuming that the P and A events are incompatible.

The particle conservation law implied in the DCM is consistently generalized to the conservation of impurity CS's moving in the 2D phase space. It is that results in a symmetric representation of transport in charge and radial variables on equal terms as suggested by the generalized FPKE. In addition, a 2D Markovian impurity equilibrium could be assumed, since it consistently follows from the so-called ergodic principle [3], while transport rates can be directly derived from the local balance of CS fluxes.

Moreover, the concept of impurity CS transport allows one to draw an unexpected conclusion about the determining role of atomic processes in impurity transport [17]. Clear evidence of this interpretation can be revealed in experiments and related modelling practice. They are:

- coronal equilibrium (CE) of heavy impurities indeed found in the early studies of Cr, Ni, and Mo impurities on the TFR tokamak [22, 23], and then confirmed by modelling practice for W on the ASDEX Upgrade tokamak [14, 15]. This meant that the equilibrium assumed by the DCM between 1D particle transport and 1D balance of ionization-recombination processes could not be observed;
– a noticeable drop in the diffusion coefficient D at the central impurity accumulation and a sharp difference between transport in the plasma core from that in the rest peripheral plasma (see, e.g., [24]) (that occurs due to the largest size in the central equilibrium cell (CEC) [17]);
– the coupling found between central accumulation of impurities and diffusion coefficient D: the greater the accumulation of the impurity in the plasma core, the lower D [17, 25], and vice versa, that is, the "flat" distribution is systematically associated with an increase D to anomalous values (in the conventional comparison with neoclassical predictions) from the core to the plasma edge;

– two characteristic maxima on the total density profiles: impurity accumulation takes place simultaneously at the edge and in the plasma core, as found, e.g., for W in JET [1, 17].

Meanwhile, the imposition of ionization-recombination on the particle transport results in a fundamental nonlinearity of transport analysis. So, the analysis of nonlinear equations of even a simplest 2D system of four charge states (two in space and two in charge called the equilibrium cell (EC)) – leads to a transcendental equation [17]. The proposed general solution can be developed based on a number of reducing 2D schemes and the use of the pseudo-state technique.

In this paper, we analyze in detail the CS equilibrium and its main dimensionless scale, constant, λ, which turns out to be common to all emerging nonlinear problems and possible reducing schemes for a given GM [17]. So, a direct relationship is established between λ, the standard transport coefficients and the impurity confinement time τ_p. An important generalization of the EC concept is developed in the form of the reduced equilibrium cell (REC). It is shown that the REC allows us to proceed directly to impurity equilibrium analysis based on a wide variety of total density profiles well known from experiments, while the impurity recombination rates are not well known as input of modeling.

The structure of the paper is as follows. In the second part, we consider possible schemes for reducing GM to easy-to-analyze simplifications. The matrix description of the reducing distribution of the total impurity density is considered in detail, and its important relationship with the GM equilibrium is shown through the scale factor λ, which is analyzed in detail in part 3. The model and results of recovery of the relative density profile of hydrogen neutrals that determine the impurity charge exchange recombination rate are given in part 4. Part 5 presents the conclusions.

2. Charge state equilibrium and transport

In the classical review of Braginsky [26], an equation representing the impurity transport was given as follows

$$\frac{\partial n_k(r,t)}{\partial t}+\nabla_r\Gamma_k(r,t)=Q_k(r,t), \tag{2}$$

where $n_k(r,t)$ is the density of impurity particles in k-th CS (k = 0, 1,..., Z), $\Gamma_k(r,t)$ is the particle flux of the k-th CS and $\sum_k Q_k(r,t)=0$. All changes of $n_k(r,t)$ due to ionization-recombination processes are described in Equation (1) by the term $Q_k(r,t)$, but the expression for it was not considered in the review. Nevertheless, it is clearly seen, that the proper phase space for Equation (2) has two independent variables, k and r (and time). Consequently, it would have to be considered in the 2D phase space of these k and r on equal terms using the system approach suggested by FPKE. In this case, the 2D transport represented in the Set (2) must also be consistently analyzed in a general series of discrete mD-Markovian processes.

2.1. The discrete transport and equilibrium conditions

In the general mD case, the differential probability distribution function $g(x_1,x_2,...,x_m)$ with independent variables $x_1,x_2,...,x_m$ can be represented by the FPKE [3-5]

$$\frac{\partial g}{\partial t}=-\sum_i\frac{\partial}{\partial x_i}\left(A_i g\right)+\sum_{i,j}\frac{\partial^2}{\partial x_i\partial x_j}\left(B_{ij}g\right), \tag{3}$$

where A_i is a vector of convective fluxes, B_{ij} is a tensor of generalized coefficients of diffusion in the mD phase space, $\int g\prod dx_i=1$. It is also assumed here that the variables x_i and x_j are changed almost continuously. The function $g(x_1,x_2,...,x_m)$ must satisfy the Smoluchowski Equation with integration over mD phase volume $\prod dx_i$. The derivation of equation (3) can be found elsewhere [4, 5]. $Q_k(r,t)$ given in Equation (2) can be directly found from comparing Equations (2) and (3).

Preprints (www.preprints.org) | NOT PEER-REVIEWED | Posted: 23 December 2020 doi:10.20944/preprints202012.0574.v1

To represent atomic processes in convenient discrete form, Equation (2) must obviously be modified. Consider the discrete 2D GM, which is usually used to discretize standard equations in transport codes [6]. We introduce a grid probability distribution function, g_{kn}, where $k = 0, 1, 2, ..., Z$ and n is the radial index instead of r; $n = 1, 2, ..., N$, $N=m+1$, where m is the number of cells. Since g_{kn} is normalized as follows $\sum_{k,n} g_{kn} = 1$, we get $\sum_{k=0}^{Z} g_{kn} = p_n$, that is, the total local (on n) normalized particle density and $\sum_{n=1}^{N} g_{kn} = q_k$, that is, the total normalized density of all ions with the same charge k. p_n and q_k are related to g_{kn} by the distribution functions f_{kn} and φ_{kn} according to

$$g_{kn} = p_n f_{kn} = q_k \varphi_{kn} \tag{4}$$

and normalizations: $\sum_{k=0}^{Z} f_{kn} = 1$, $\sum_{n=1}^{N} \varphi_{kn} = 1$.

The CS dynamics on the grid are considered as the random jumps to neighboring positions (grid nodes): by k due to a-transport and/or by n due to p-transport. The a-transport rates are S_{kn} and R_{kn}, that is, the rates of ionization and recombination. The p-transport rates (also in s^{-1}) could be denoted as w^p_{kn} if the CS motion by p-transport is directed from n to $n+1$ and as u^p_{kn+1} if the motion is directed from $n+1$ to n.

The discrete 2D form of Equation (3) assumes the choice of the necessary system of pairwise incompatible events (in accordance with the general probability summation formula) associated with states without matching indices. Therefore, we consider pairs of diagonally conjugate states: *(k, n)* and *(k+1, n+1)*; *(k+1, n)* and *(k, n+1)* and the corresponding diagonal rates w_{kn}, u_{k+1n+1} and w'_{k+1n}, u'_{kn+1}. Then the 2D equation (for example, for the first of the symmetric pairs) is obtained as

$$\frac{\partial g_{kn}}{\partial t} = u_{k+1n+1} g_{k+1n+1} - \left(w_{kn} + u_{kn}\right) \cdot g_{kn} + w_{k-1n-1} g_{k-1n-1}, \tag{5}$$

where the rate matrix is tridiagonal, Jacobian, singular (it has zero value in the spectrum of its real eigenvalues) and similar to some symmetric real matrix. At any time, t, of the temporal evolution of the Set (5), there is an ergodic limit (see [3]), which is determined by a complete set of these matrices. The stationary solution of Equation (5) is simultaneously the local equilibrium condition

$$\begin{aligned} w_{kn} g_{kn} &= u_{k+1n+1} g_{k+1n+1}, \\ w'_{k+1n} g_{k+1n} &= u'_{kn+1} g_{kn+1}. \end{aligned} \tag{6}$$

The 2D equilibrium is symmetric, assuming the equalities of symmetric pairs of counter CS fluxes

$$\begin{aligned} w^p_{kn} g_{kn} &= u^p_{kn+1} g_{kn+1}, \\ S_{kn} g_{kn} &= R_{k+1n} g_{k+1n}, \end{aligned} \tag{7}$$

which can be proved strictly in general for any 2D structures (see in [17]). Therefore, note, that Equations (6) directly follow from these Equalities (7) and independent of Equation (5).

The nonlinearity of the problems that arise in the analysis of the CS transport is directly follows from Equations (6) and (7). So, we get

$$\frac{g_{k+1n+1}}{g_{kn}} = \frac{w^p_{k+1n} S_{kn}}{u^p_{k+1n+1} R_{k+1n}} = \frac{w^p_{kn} S_{kn+1}}{u^p_{kn+1} R_{k+1n+1}} = \frac{c_1 w^p_{k+1n} S_{kn} + c_2 w^p_{kn} S_{kn+1}}{c_1 u^p_{k+1n+1} R_{k+1n} + c_2 u^p_{kn+1} R_{k+1n+1}}, \tag{8}$$

where c_1 and c_2 are arbitrary constants to be found. By defining

$$\begin{aligned} w_{kn} &\equiv c_1 w^p_{k+1n} S_{kn} + c_2 w^p_{kn} S_{kn+1}, \\ u_{k+1n+1} &\equiv c_1 u^p_{k+1n+1} R_{k+1n} + c_2 u^p_{kn+1} R_{k+1n+1}, \end{aligned} \tag{9}$$

Preprints (www.preprints.org) | NOT PEER-REVIEWED | Posted: 23 December 2020 doi:10.20944/preprints202012.0574.v1

we obtain the general case of conditions (6) expressed in terms of products of conditional probabilities of particle and charge transport processes. Formally, using the normalization of g_{kn} with Equations (8-9), we obtain the set of rate equations. But even simplest expressions for the diagonal CS transport in the single EC give a strong nonlinear relationship between the probability distribution and transport rates (see, e.g., the Set (13) below or Formula (21) in [17]).

Thus, the rates $\{w^p_{kn}\}, \{u^p_{kn}\}$ and $\{S_{kn}\}, \{R_{kn}\}$ are related in a nonlinear way to $\{w_{kn}\}, \{u_{kn}\}$ in accordance with Formulas (1) and (5-9). Using Formulas (4), Equalities (7) can be rewritten as

$$\begin{aligned} w^p_{kn}\varphi_{kn} &= u^p_{kn+1}\varphi_{kn+1}, \\ S_{kn}f_{kn} &= R_{k+1n}f_{k+1n}. \end{aligned} \tag{10}$$

where both distribution functions are normalized (see after Formula (4)), hence the double Set (10) can be interpreted as a generalized equilibrium or double coronal equilibrium (DCE). For each cell, there are symmetric pairs of such equalities that define the local DCE conditions. A local unit of phase volume has a pair of necessary transport ratios, as shown in Figure 1.

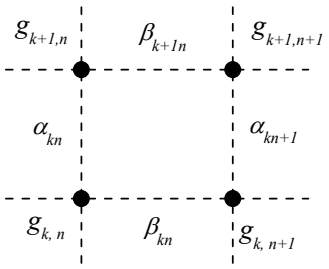

Figure 1. A separate cell of GM with the ratio of rates between nodes.

Each impurity particle within a local unit of the discrete phase space is characterized by four states. Consider the relationships: $\alpha_{kn} = S_{kn} / R_{k+1n} = g_{k+1n} / g_{kn}$ and $\beta_{kn} = w^p_{kn} / u^p_{kn+1} = g_{kn+1} / g_{kn}$. Using the entered relations, the conditions (7) and (10) can be rewritten again as follows

$$\frac{\alpha_{kn}}{\alpha_{kn+1}} = \frac{\beta_{kn}}{\beta_{k+1n}}, \tag{11}$$

where both values in the left part obviously depend only on the rates of ionization and recombination and relate only to *a*-transport, while in the right part – only to *p*-transport. Expression (11) defines the impurity equilibrium as the necessary local coupling of *a*- and *p*-transports within each cell. A transport that satisfies the condition (11) could be called an equilibrium transport.

Whatever the mechanisms of *p*-transport in the plasma (collisional or turbulent), local equilibrium of impurities can only be provided by the equilibrium *p*-transport rates. Consequently, the local equilibrium transport is determined by statistically independent rates of ionization and recombination. Since the *p*-transport corresponds to the *a*-transport, that is, it turns out to be equilibrium, a generalized DCE of impurity (10-11) occurs.

Thus, local EC is simultaneously: (i) a unit phase space volume and the characteristic scale of the local equilibrium, (ii) self-consistent equilibrium system, which provides a comprehensive analysis of the rate ratios of *a*- and *p*-transports, (iii) a crucial tool for analyzing a general equilibrium of impurity CS transport.

The condition (11) couples only the rate ratios, which can be reproduced for impurities with different Z and with significantly different rates. But only they determine the equilibrium transport along with the resulting stationary density distributions. The corresponding similarities of the equilibrium rate ratios can be suspected in experiments, e.g., when there is an apparently similar stationary density profiles of the central accumulation of C [27, 28], Ar [29, 30] and W [1, 31].

Contrary, the absolute values of the atomic rates determine the equilibrium scale, λ, that is, an equilibrium constant of steady state impurity [17]. It turns out to be the same to all cells and

Preprints (www.preprints.org) | NOT PEER-REVIEWED | Posted: 23 December 2020 doi:10.20944/preprints202012.0574.v1

reducing GM schemes, as will be shown below. Therefore, the difference in the equilibrium of impurities appears primarily as a function $\lambda(Z)$, which strongly depends on the atomic structure and the rates of the most abundant ions. For light and mid-Z impurities, these are K- and L-shells of *H-*, *He-* and *Li*-like ions. Normalizing the atomic rates by this λ allows us to develop a generalized elementary 2D model of equilibrium that could be called a reduced equilibrium cell (REC). Formally the REC is just a special case of the EC with λ =1.

2.2. Reduced equilibrium cell

The CS equilibrium and transport in the EC is completely determined by the rates of ionization and recombination processes, S_1, S_2 and R_1, R_2 respectively. The EC scheme is shown in Figure 2.

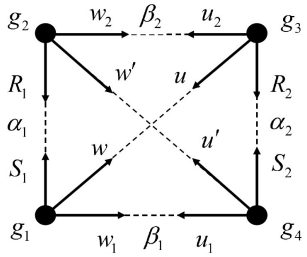

Figure 2. Scheme of the equilibrium cell.

The relations $\alpha_1 = S_1 / R_1$, $\alpha_2 = S_2 / R_2$, $s = S_2 / S_1$, $\tilde{r} = R_2 / R_1$, $\beta_1 = w_1 / u_1$, $\beta_2 = w_2 / u_2$ are either directly obtained from the given rates of atomic processes, or can be obtained from the equilibrium analysis. In particular, in the case of the EC the condition (11) is

$$\gamma \equiv \frac{\alpha_2}{\alpha_1} = \frac{\beta_2}{\beta_1} = \frac{s}{\tilde{r}}. \tag{12}$$

Solutions of the equations describing the temporal evolution of densities $p_{1/2} = g_{1/3} + g_{2/4}$, $q_{1/2} = g_{1/2} + g_{4/3}$, $g_{1/3}$, $g_{2/4}$ (for short, the subscripts for pairs are changed) include non-zero eigenvalues of the EC matrix equations. As was shown in the EC analysis [17], these turn out to be equal, i.e. $\lambda = \lambda' = \lambda_p = \lambda_q$, where $\lambda = w + u$, $\lambda' = w' + u'$ are the constants of the diagonal balance as follows from the FPKE adopted for the EC, $\lambda_p = \bar{w} + \bar{u}$, where $\bar{w} = (w_1 + w_2\alpha_1)/(1+\alpha_1)$, $\bar{u} = (u_1 + u_2\alpha_2)/(1+\alpha_2)$, and $\lambda_q = \bar{S} + \bar{R}$, where $\bar{S} = (S_1 + S_2\beta_1)/(1+\beta_1)$ and $\bar{R} = (R_1 + R_2\beta_2)/(1+\beta_2)$.

Now consider the REC, in which, as noted above, all rates are normalized to λ, that is, $\tilde{S}_1 = S_1 / \lambda$, $\tilde{S}_2 = S_2 / \lambda$, $\tilde{R}_1 = R_1 / \lambda$ and $\tilde{R}_2 = R_2 / \lambda$. From ratios we also get that $\tilde{w}_1 = w_1 / \lambda$, $\tilde{w}_2 = w_2 / \lambda$ and $\tilde{u}_1 = u_1 / \lambda$, $\tilde{u}_2 = u_2 / \lambda$. The definition of the REC is a set of equalities $\lambda = \lambda' = \lambda_p = \lambda_q = 1$. The basic equations derived for the EC are the same for the REC also:

$$\begin{aligned} &1 + \kappa' x v = \frac{x}{x_e} + \frac{v}{v_e}, \\ &x + v = \frac{(1+\kappa')}{s}\frac{(1+\alpha_1)(1+\alpha_2)}{(1+\beta_1)(\alpha_1+\alpha_2\beta_1)}, \\ &\frac{x}{1+\kappa' x} + \frac{v}{1+v} = \frac{\alpha_2}{(1+\alpha_2\beta_1)}\cdot\frac{(1+\kappa')}{s}\cdot\frac{(1+\alpha_1+\beta_1+\alpha_2\beta_1)}{(1+\beta_1)(\alpha_1+\alpha_2\beta_1)}, \end{aligned} \tag{13}$$

where $v(x=0) \equiv v_e = (\kappa - 1)/(\kappa' - \kappa)$, $x(v=0) \equiv x_e = (\kappa - 1)/(1 - \kappa'\kappa)$ in the notations $x = u_2 / R_2 = \tilde{u}_2 / \tilde{R}_2$, $v = u_1 / S_2 = \tilde{u}_1 / \tilde{S}_2$, $\kappa' = \beta_1 s$, $\kappa = \alpha_2(1 + \beta_1/\alpha_1)/(1+\alpha_2\beta_1)$ and $\tilde{w}_1 = \beta_1\tilde{u}_1$ ($w_1 = \beta_1 u_1$), $\tilde{w}_2 = \beta_2\tilde{u}_2$ ($w_2 = \beta_2 u_2$). Then we add to Equations (13) two expressions for $\alpha_1(p, \beta_1)$ and

 doi:10.20944/preprints202012.0574.v1

$\alpha_2(p,\beta_1)$ (where $p \equiv p_2/p_1$) taken from the equation $\lambda_q = \bar{S} + \bar{R} = 1$ and the relation $p = \beta_1(1+\alpha_2)/(1+\alpha_1)$ as follows

$$\begin{aligned} \alpha_1 &= \frac{(1+\beta_1)^2}{(1+p)(1+\beta_1-\tilde{S}_1-\tilde{S}_2\beta_1)} - 1 \\ \alpha_2 &= \frac{p}{\beta_1}(1+\alpha_1) - 1 \end{aligned} . \tag{14}$$

The final equation, which is obtained from the Set (13-14), has the form

$$\Phi_P(\tilde{S}_1, \tilde{S}_2, p, \beta_1) = 0, \tag{15}$$

where the values $\tilde{S}_1, \tilde{S}_2, p$ are assumed to be given. Equation (15) differs from that for the EC [17]

$$\Phi_S(\alpha_1, \alpha_2, s, \beta_1) = 0, \tag{16}$$

which can be resolved with respect to β_1 for a given α_1, α_2, $s = S_2/S_1 = \tilde{S}_2/\tilde{S}_1$. An equilibrium with a given ionization base of the cell, *s*, could be called an *S*-equilibrium.

The symmetric version of the EC can be based on recombination processes (for given α_1 and α_2). This *R*-equilibrium is given by a triple $\alpha_1^{-1}, \alpha_2^{-1}, \tilde{r}$ with other final Equation

$$\Phi_R(\alpha_1^{-1}, \alpha_2^{-1}, \tilde{r}, \beta_1) = 0. \tag{17}$$

It is important to note that the solution β_1 of Equations (15-17) is not a continuous function, since in general there are two equilibrium regions defined by the following inequalities

$$\kappa' < \kappa < 1, \tag{18}$$

and

$$\kappa' < 1 < \kappa. \tag{19}$$

The transition between regions (18) and (19) occurs by a jumps in p, x and v (see Figure 5 in [17]) at the bifurcation points of Equations (15-17). These points are the boundaries of the regions (18-19).

For other elementary equilibrium schemes involving one or more cells, the solutions of the final problems (16) and (17) coincide in principle. However, real impurity equilibrium systems in a plasma with different equilibrium bases (*S* or *R*) can differ significantly by their equilibrium rate profiles and by the conditions that implement the equilibrium at the variable boundaries. The point is that any of the three options is possible: (i) when the equilibrium can have both bases and different profiles, (ii) when only one of the two equilibrium options is realized, and, finally, (iii) when there is no equilibrium for given distributions of parameters. Thus, the modelling shows that the complex cases turn out to have different bases of equilibrium and boundary conditions.

Thus, the solution of problem (15) can be used to model the CS equilibrium, which exactly corresponds to the given (or known from experiments) profiles of the total impurity density with known ionization rates. The modelling using this approach are considered below. However, in contrast to the settings of the direct problems (16) and (17), which provide the constant scale λ, the problem (15) assumes that λ is already known, e.g., from approximate estimates (which are discussed below) or from a preliminary approximate calculation of the equilibrium.

Direct calculations of the equilibrium of the Ar impurity in the JET tokamak showed [17] that the last cell in the CCs differ from the ithers in a number of important properties. So, for *m*-th cell we get $\alpha_2(EC) = \alpha_{jm+1}(CCs)$ in the region (19). We also obtain that $\gamma \equiv \alpha_2/\alpha_1 >> 1$, $s >> 1$, $\beta_1 << 1$. Typical values are γ = 20-100, s = 4-20, $\beta_1 = w_1/u_1$ = $2\cdot10^{-4} - 2\cdot10^{-3}$. In this case, the analysis can be simplified and, in fact, gives the position of the impurity equilibrium boundary. In the region (19), it turns out that $\kappa \approx \alpha_2$, $v << x \approx 1/\tilde{R}_2$, $\tilde{S}_1 \approx 1/(1+p)$.

Preprints (www.preprints.org) | NOT PEER-REVIEWED | Posted: 23 December 2020 doi:10.20944/preprints202012.0574.v1

Further, the analysis of the equilibrium in the last EC allows us to calculate the limit values of the boundary densities that satisfy the simple criterion $v \approx 0$ for several values of γ as a function $p(s, v=0)$. Figure 3 shows the dependence of the limit ratio of densities in the last EC. The equilibrium for a denoted value γ is possible only at densities higher than the calculated limit values.

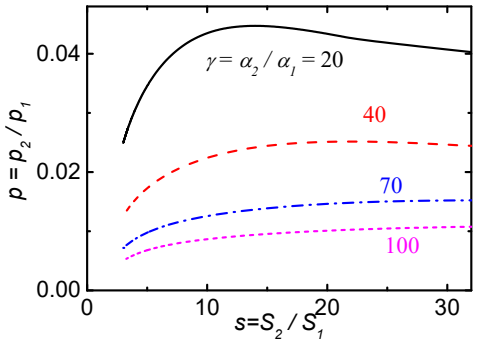

Figure 3. Dependence of the limit ratio of densities in the boundary EC under the condition of the ionization rate gradient in this cell.

2.3. Reduction schemes

The Markovian equilibrium, assumed in GM for stationary plasma conditions, allows us to find the equilibrium transport by reducing GM by the pseudo-state technique. The main reducing schemes are shown in Figure 4.

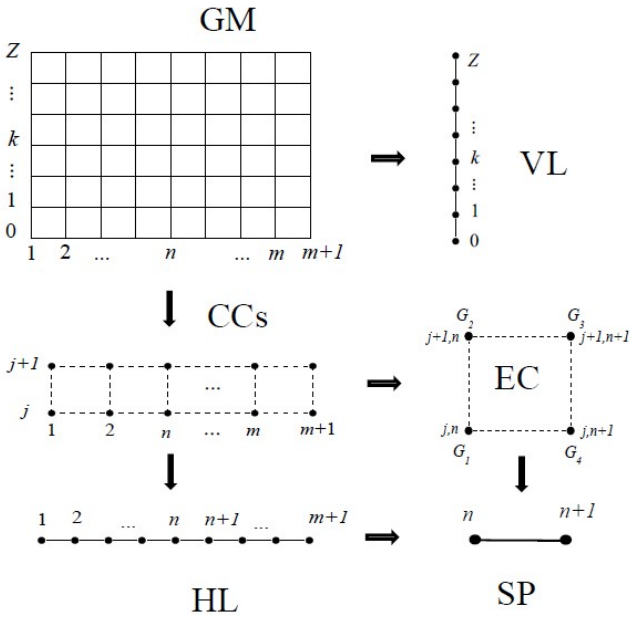

Figure 4. The main schemes of GM reduction by the pseudo-state technique: GM – the initial grid model of impurity distributions, CCs – coupled cells, HL and VL denote horizontal and vertical CS lines, respectively, EC - an equilibrium cell, SP - a separate pair.

The most obvious reduction options are local summations of the initial grid distribution function g_{kn} for each n and for each k. It is easy to find several reducing schemes where the nodes are convenient simple sums of CS's that preserve the original density distribution $\{p_n\}$ with the normalization. Thus, the formal algebraic procedure allows to reduce the analysis of nonlinear rate transport equations to the solution of a single transcendental equation of the form (15), (16) or (17).

Preprints (www.preprints.org) | NOT PEER-REVIEWED | Posted: 23 December 2020 doi:10.20944/preprints202012.0574.v1

So, the GM equilibrium can be successively reduced to a local equilibrium of just four pseudo-states of EC, which are the sums of the corresponding GM quadrants around the single nodes of local EC, that is $G_i = \sum_i g_{kn}$, where i =1, 2, 3, 4 with normalization preserved $\sum_i G_i = 1$.

Invariance of the resulting distributions can be illustrated by comparing densities, for example, in simple schemes HL, EC, and SP, where they are connected by obvious equalities

$$\begin{aligned} \sum_{i=1}^{n} p_i\left(HL\right) &= P_1(SP) = P_1(EC) = G_1(EC) + G_2(EC), \\ \sum_{i=n+1}^{m+1} p_i\left(HL\right) &= P_2(SP) = P_2(EC) = G_3(EC) + G_4(EC). \end{aligned} \tag{20}$$

So, for the CCs and HL, the density distribution $\{p_n\}$ is common, i.e., a reduction invariant. In the same way, the horizontal (HL) and vertical (VL) lines of pseudo-states preserve $\{p_n\}$ and $\{q_k\}$ distributions common with the original GM (see Expressions (3) and (4)). Summation of Equations (5) results in the following set of the HL

$$\frac{\partial p_n}{\partial t} = u_{n+1} p_{n+1} - \left(u_n + w_n\right) p_n + w_{n-1} p_{n-1}, \tag{21}$$

where $u_n = \sum_{k=0}^{Z} u_{kn}^{p} f_{kn}$ and $w_n = \sum_{k=0}^{Z} w_{kn}^{p} f_{kn}$, but for the VL to a similar set

$$\frac{\partial q_k}{\partial t} = R_{k+1} q_{k+1} - \left(R_k + S_k\right) q_k + S_{k-1} q_{k-1}, \tag{22}$$

where $R_k = \sum_{n=1}^{N} R_{kn} \varphi_{kn}$ and $S_k = \sum_{n=1}^{N} S_{kn} \varphi_{kn}$.

Another important invariant of the reduction is the CS fluxes between the original neighboring states and their reducing pseudo-states. In this case, the changed transition rates between all new nodes must correspond to the pseudo-state densities. The equalities of probabilistic fluxes determine these rates between pseudo-states. The SP and EC rates are related to each other as follows

$$\begin{aligned} w \cdot P_1 &= w_1 G_1 + w_2 G_2, \\ u \cdot P_2 &= u_1 G_4 + u_2 G_3. \end{aligned} \tag{23}$$

Obviously, in the case of the CCs scheme, the proper equilibrium is generally provided by the correct choice of the j and j+1 levels of ionic charge k. It is seen that the choice is determined by the most abundant impurity ions in the plasma, i.e. their corresponding charge and external atomic levels. These j and j+1 could be called the equilibrium levels of steady state impurity.

The first stage of the GM reduction to the CCs is the summation along vertical lines below and above the levels $j / j+1$ respectively. The resulting CCs pseudo-states are the following sums

$$G_{jn} = \sum_{k=0}^{j} g_{kn}, \; G_{j+1n} = \sum_{k=j+1}^{Z} g_{kn}. \tag{24}$$

The fluxes between levels $j / j+1$ in the original and reducing schemes are assumed to remain unchanged, which allows us to find the rates

$$S_{jn} = S_{kn} g_{kn} / G_{jn}, R_{j+1n} = R_{k+1n} g_{k+1n} / G_{j+1n}. \tag{25}$$

The sequence of ratios (25) from the sums (24) can be called the equilibrium function

$$\alpha_{jn} = G_{j+1n} / G_{jn} = S_{jn} / R_{j+1n}, \tag{26}$$

which determines $f_{jn}\left(\{\alpha_{jn}\}\right)$ and similarly the function $\varphi_{jn}\left(\{\beta_{jn}\}\right)$, since

$$\beta_{jn} = G_{jn+1} / G_{jn}. \tag{27}$$

Preprints (www.preprints.org) | NOT PEER-REVIEWED | Posted: 23 December 2020 doi:10.20944/preprints202012.0574.v1

Besides the density distribution and CS fluxes between neighboring states of original scheme there is another important reduction invariant. It is the equilibrium constant λ discussed in detail in the next section.

3. Equilibrium constant

The reduction invariants allow us to obtain a general solution to the original transport nonlinear problem. But there is a common for all reducing schemes and, therefore, the most important equilibrium invariant given by the value λ, which should be considered in detail.

Averaging the atomic rates and its ratios over the corresponding φ functions for the n-th reducing EC and for levels $j / j+1$ of CCs, we get

$$\begin{aligned} \overline{S}(n) &= \frac{S_1(n)+\beta_1(n)S_2(n)}{1+\beta_1(n)} = \sum_{n=1}^{m+1} S_{jn}\varphi_{jn}, \\ \overline{R}(n) &= \frac{S_1(n)+\beta_1(n)S_2(n)}{\alpha_1(n)+\alpha_2(n)\beta_1(n)} = \sum_{n=1}^{m+1} R_{j+1n}\varphi_{j+1n}, \\ \overline{\alpha} &= \overline{S}(n)/\overline{R}(n) = \frac{\alpha_1(n)+\alpha_2(n)\beta_1(n)}{1+\beta_1(n)}. \end{aligned} \tag{28}$$

It is seen that $\overline{S}(n)$ and $\overline{R}(n)$ remain the same for all reducing cells of the CCs. Then the sum

$$\lambda(n) = \overline{S}(n) + \overline{R}(n) \tag{29}$$

is also a common constant. The same conclusions can be drawn in the symmetric case

$$\lambda(k) = \overline{w}(k) + \overline{u}(k). \tag{30}$$

The intersection of vertical and horizontal reducing lines and imposed of the EC's (with the corresponding pairs of n and k) reveals that for any reducing local EC there is only a single common constant $\lambda(n) = \lambda(k) = \lambda$. Note that the non-zero eigenvalues of all reducing SP are also equal to λ. In other words, λ is a constant, that determines all possible cases of impurity equilibrium in GM.

The important relationship between λ and the equilibrium transport rates, density distributions, $\{p_n\}$, and, finally, the characteristic times of the impurity confinement, τ_p, can be found as follows.

3.1. Time scale of transport rates

In the case of steady state equilibrium ($\partial p_n / \partial t = 0$), the solution of the set (21) is determined by the equalities of the same particle fluxes from neighboring pseudo-states. Comparing these fluxes for HL and SP and using Equation $\lambda = w + u$, we obtain equalities correspond to the conservation of fluxes for each pair of n and n+1 states of HL and the sequence of pseudo-states of SP:

$$\begin{aligned} & w(n) + u(n+1) = \lambda, \\ & p_n w_n = \sum_{i=1}^{n} p_i \cdot w(n) = p_{n+1} u_{n+1} = \sum_{i=n+1}^{m+1} p_i \cdot u(n+1), \end{aligned}' \tag{31}$$

that gives a complete set of equations. The solution can be expressed as follows

$$\begin{aligned} w_n &= \lambda \cdot \tilde{w}_n \\ u_{n+1} &= \lambda \cdot \tilde{u}_{n+1} \end{aligned}', \tag{32}$$

where $\tilde{w}_n$ and $\tilde{u}_{n+1}$ are the reduced particle transport rates:

Preprints (www.preprints.org) | NOT PEER-REVIEWED | Posted: 23 December 2020 doi:10.20944/preprints202012.0574.v1

$$\tilde{w}_n = \sum_{i=1}^{n} p_i \left(1 - \sum_{i=1}^{n} p_i\right) / p_n,$$
$$\tilde{u}_{n+1} = \sum_{i=1}^{n} p_i \cdot \left(1 - \sum_{i=1}^{n} p_i\right) / p_{n+1}. \quad (33)$$

Using Expressions (32), Equation (25) can be rewritten

$$\frac{\partial \vec{p}}{\partial t} = N \cdot \vec{p} = \lambda \cdot \tilde{N} \cdot \vec{p}\,, \quad (34)$$

where N is the matrix of Equation (25), $\tilde{N}$ is the reduced matrix combined from the elements (33):

$$\tilde{N}\left(\{p_n\}\right) = \begin{vmatrix} -\tilde{w}_1 & \tilde{u}_2 & 0 & 0 \\ \tilde{w}_1 & -\left(\tilde{w}_2 + \tilde{u}_2\right) & \tilde{u}_3 & \dots \\ \dots & \dots & \dots & \tilde{u}_{m+1} \\ 0 & \dots & \tilde{w}_m & -\tilde{u}_{m+1} \end{vmatrix} = B^{-1} T \cdot \begin{vmatrix} 0 & 0 & \dots & 0 \\ 0 & -\lambda_1 & \dots & 0 \\ \dots & \dots & \dots & 0 \\ 0 & \dots & 0 & -\lambda_m \end{vmatrix} \cdot T^t B\,, \quad (35)$$

where $\{0, \lambda_1, \lambda_2, ..., \lambda_m\}$ is the spectrum of its absolute eigenvalues (let $0 < \lambda_1 < \lambda_2 < ... < \lambda_m$), determined by the density profile according to Formula (33), the matrix B is diagonal, and T is orthogonal, and T^t is the transposed orthogonal matrix (see, e.g., in [19]).

Thus, the value λ determines the scale $\tau = \lambda \cdot t$ of temporal evolution $\{p_n(\tau)\}$. The eigenvalues of $\tilde{N}$ is related only to the stationary profile $\{p_n\}$, as follows from Formulas (33-35).

3.2. Impurity equilibrium and transport coefficients

The discrete structure of CS transport, finite equilibrium regions, and bifurcations during transitions between them strongly limit the possibility of describing impurity transport by differential equations that require continuity of the corresponding functions along with their derivatives in the entire domain of definition. On the contrary, the proposed matrix approach uses a minimum of input information to analysis and most closely corresponds to the physical nature of probabilistic (random) CS transport. Indeed, Equations (21) and (34) represent a matrix analogue of the standard 1D continuity equation for the total impurity density

$$\frac{\partial n_Z(r,t)}{\partial t} + \nabla_r \Gamma_Z(r,t) = 0\,, \quad (36)$$

where $\Gamma_Z(r,t) = \sum \Gamma_k(r,t)$. Note that for a stationary impurity profile $n_Z(\rho)$ obtained in experiment, the corresponding discrete profile $\{p_n\}$ is also well known, since $\partial \ln p_n / \partial \rho = \partial \ln n_Z / \partial \rho$, where $\rho = r/a$, a is the minor radius of the plasma column. Next, we note that in the accepted cylindrical geometry, it is convenient to set $\rho^2 = n/N$ in accordance with Equation (21), and then $N = 2(m+1)$. Comparing the coefficients before the second derivatives in expressions (21) (after expanding by n as a continuous parameter, see, e.g., in [17]) and (36) and using the relations (32), we obtain the particle diffusion coefficient, D, in the form

$$D = \frac{a^2}{8(m+1)^3} \lambda \tilde{D}\,, \quad (37)$$

where $\tilde{D}\left(\{p_n\}\right) = \left(\tilde{w}_n + \tilde{u}_n\right)/2$ is a reduced diffusivity, which is easily calculated on Formulas (33). The reduced convective velocity, $\tilde{v}$, is obtained by a standard way $\tilde{v} = \tilde{D}/a \cdot \partial \ln p_n / \partial \rho$.

The strong dependence $D \propto (m+1)^{-3}$ occurs in Formula (37) for several reasons. First, using the expansion in series on n of the Set (21) we get the second derivative depending on n with corresponding coefficient (see, e.g., in [17-19]). Second, the comparison can only be made using the

 doi:10.20944/preprints202012.0574.v1

initially accepted cylindrical coordinate system with argument $\rho^2 = n/(m+1)$, which provides a correct description of the radial states (layers) with equal plasma volumes. Third, unlike (36), the sets (21) and (34) are linear on *n*. But the argument ρ^2 appears before the second derivative in the steady state solution of Equation (36), that is, in the confluent hypergeometric equation to be solved (see, for example, in [21, 33-35]). Then, to convert the original coefficient before second derivative of linear expression (21) into that of the standard Equation (36) with that required ρ^2, it is necessary to include the correcting scale factor $(m+1)^{-1}$ into the expression of *D*, since the factor n is just included in the diffusivity profile $\tilde{D}(n)$.

Now we can directly calculate the reduced transport profiles $\tilde{D}$ and $\tilde{v}$ together with the profiles $\{\tilde{w}_n\}$ and $\{\tilde{u}_n\}$ corresponding to the given profile $n_Z(\rho)$. We can directly derive $\{w_n\}$ and $\{u_n\}$, $\{\tilde{w}_n\}$ and $\{\tilde{u}_n\}$ using the invariance of pseudo-state fluxes of HL and EC systems:

$$\begin{aligned} p_n w_n &= G_1(n) w_1(n) + G_2(n) w_2(n) \\ p_{n+1} u_{n+1} &= G_3(n) u_2(n) + G_4(n) u_1(n) \end{aligned}, \tag{38}$$

where for each *n* we can use the following obvious expressions

$$\begin{aligned} &G_1 = 1/(1+\alpha_1+\beta_1+\alpha_2\beta_1), G_2 = \alpha_1/(1+\alpha_1+\beta_1+\alpha_2\beta_1), \\ &G_3 = \alpha_2\beta_1/(1+\alpha_1+\beta_1+\alpha_2\beta_1), G_4 = \beta_1/(1+\alpha_1+\beta_1+\alpha_2\beta_1), \end{aligned}, \tag{39}$$

$$\begin{aligned} w_1 &= S_2\beta_1 \cdot \mathrm{v},\ w_2 = \frac{S_2\beta_1}{\alpha_1} \cdot x, \\ u_1 &= S_2 \cdot \mathrm{v},\ u_2 = \frac{S_2}{\alpha_1} \cdot x, \end{aligned}, \tag{40}$$

then from Equation (13) and (38-40) we get the relations of the HL and EC values

$$\begin{aligned} w_n &= \frac{S_2\beta_1(x+v)}{p_n(1+\alpha_1+\beta_1+\alpha_2\beta_1)}, \\ u_{n+1} &= \frac{S_2\beta_1(x+v)}{p_{n+1}(1+\alpha_1+\beta_1+\alpha_2\beta_1)}. \end{aligned} \tag{41}$$

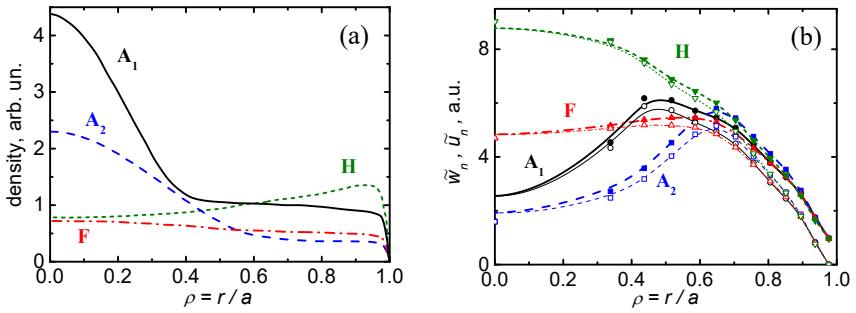

Figure 5. (a) Typical total impurity density profiles (A_1, A_2 denote accumulation, F – almost flat, H – hollow) obtained in experiments on the DIII-D [27] (A_1 for C), JT-60 [28] (A_2 for C) and JET [29, 30, 32] (A1, A2, F, H for Ar) tokamaks; (b) reduced velocity profiles $\tilde{w}_n$ (dashed) and $\tilde{u}_n$ (dotted) calculated using Formulas (33).

Typical profiles $n_Z(\rho)$, for example, of C and Ar are well known from experiments (see, e.g., in [27-32]). The profiles $n_Z(\rho)$ can be (i) peaked in the plasma core, (ii) almost flat, or (iii) slightly hollow. Figure 5 (a) shows these typical profiles observed in experiments, and Figure 5(b) shows the corresponding profiles $\{\tilde{w}_n\}$ and $\{\tilde{u}_n\}$ calculated on Formulas (33).

Preprints (www.preprints.org) | NOT PEER-REVIEWED | Posted: 23 December 2020 doi:10.20944/preprints202012.0574.v1

Numerically $\tilde{w}_n$ and $\tilde{u}_n$ close to each other in almost the entire profile. So, we conclude that $\tilde{D} \approx \tilde{w}_n \approx \tilde{u}_n$ (see Formula (37)). The closer to the center of the plasma, the better the approximate ratio is reproduced. The profiles A_1 and A_2 with central accumulation correspond to a decrease in D in the plasma core, which is in qualitative agreement with the experiments [25] and modelling [17].

3.3. Impurity equilibrium and confinement time

The confinement time of impurity particles, τ_p, is conventionally determined by the smallest of the eigenvalues of the divergence operator [33, 34], which represents the particle transport in the standard Equation (36). In the proposed matrix case, the analogue of this value, as follows from Formulas (34-35), is the product $\lambda \cdot \lambda_1$. We denote $\lambda_E \equiv \lambda_1$ the smallest (non-zero) absolute eigenvalue of the spectrum of the matrix $\tilde{N}$ (see explanation to Formula (35)). Then λ_E can be found from the spectral decomposition $\{0, \lambda_1, \lambda_2, ..., \lambda_m\}$ of the matrix $\tilde{N}(\{p_n\})$ constructed by Formulas (32-33). Using this matrix approach, we obtain a relationship between λ_E and m. Figure 6 shows the calculations of these dependencies $\lambda_E(m)$ for the profiles $n_Z(\rho)$ shown in Figure 5 (a).

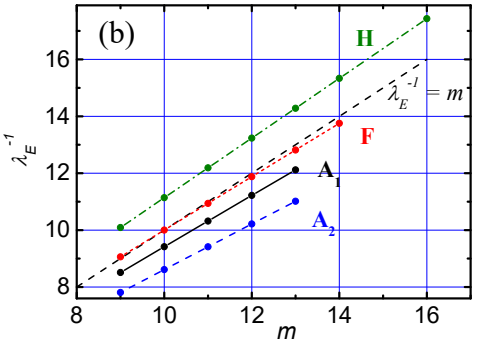

Figure 6. Dependences of the smallest (in absolute value) non-zero eigenvalue of the matrices $\tilde{N}$, corresponding to the profiles $n_Z(\rho)$ in Figure 5 (a), on the number of m cells.

From the definition of τ_p, Formulas (34-35) and calculations shown in Figure 6, we get, that

$$\tau_p = 1/(\lambda \cdot \lambda_E) \approx m/\lambda, \quad (42)$$

where the last approximate ratio is performed within a good accuracy, especially for flat (F) density profiles. From Formulas (37) and (42) we conclude that $D \propto \lambda \propto \tau_p^{-1}$. The resulting estimates of the value τ_p for the various cases of equilibrium of C and Ar impurities are presented below.

3.4. Types of impurity CS equilibrium

The atomic structure of impurity ions is directly manifested in their CS equilibrium. From Formulas (28-29), it is seen that change in the equilibrium levels $j / j+1$ can affect both λ and α_{jn}. An additional factor here is, as mentioned above, the type of the equilibrium base – ionization (S) or recombination (R). This can be shown by modelling of impurity equilibrium.

Figure 7 shows calculations (by the TICS code [17]) of the argon impurity equilibrium for the temperature and density profiles typical for a variety of discharge conditions in JET [29, 30, 32], in particular, for a plasma with $T_e(0) = 4$ keV, $T_i(0) = 4$ keV, and $n_e(0) =$ 4.5 10^{19} m^{-3}. The selected profiles of temperatures, electron density, and relative density of hydrogen neutrals $\xi_n = n_n / n_e$ remain the same as previously used for modeling Ar transport in JET.

 doi:10.20944/preprints202012.0574.v1

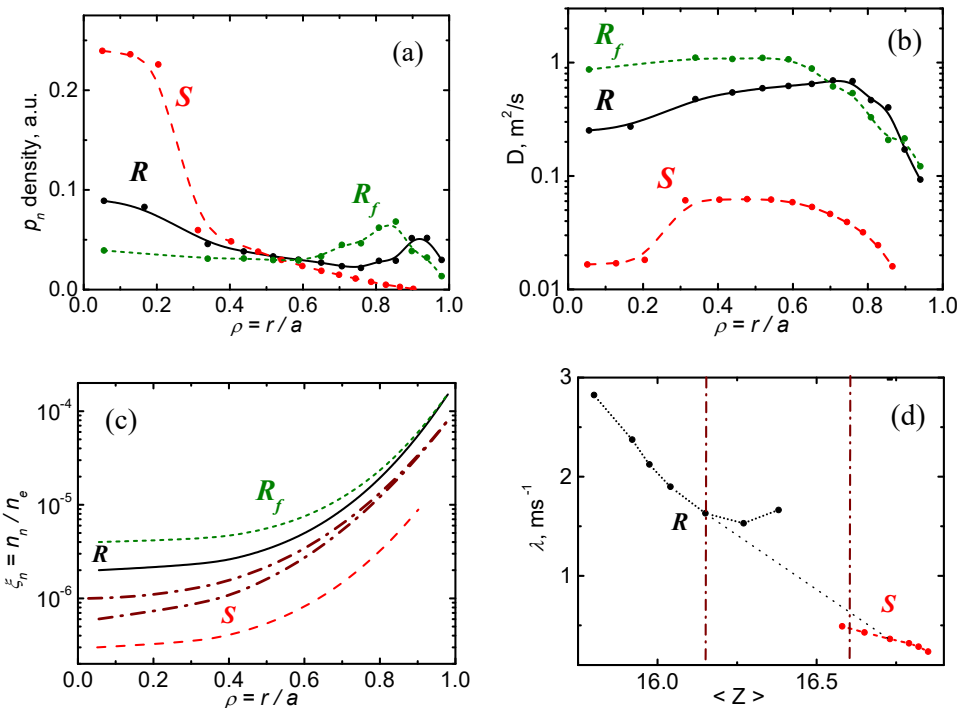

Figure 7. The equilibrium of Ar calculated with a recombination (*R*, R_f curves) and ionization (*S* curves) equilibrium base: (a) profiles with and without central accumulation; (b) profiles of the diffusivity calculated by Formula (37); (c) *S*- and *R*-equilibrium regions determined by the relative profiles of hydrogen neutrals $\xi_n = n_n / n_e$ separated by dash-dotted curves showing the limits of the transition region; (d) abrupt change in the equilibrium constant depending on the average impurity charge with a gradual transition between the *R* and *S* regions due to changes in the profiles $\xi_n(\rho)$. The dash-dotted curves on (d) show the same limits of the transition region.

Figure 7 (a) shows the profiles of the total argon density for three typical cases of the equilibrium observed in experiments. Here, discrete data points are connected by splines. The first profile, denoted by S, is a strongly peaked and obtained in the case of *S*-equilibrium with the base $j / j+1$ for *He*/*H* - like ions. The next profile denoted by R has two maxima (at the center and at the edge), calculated for *R*-equilibrium with the base $j+1/j$ for *He*/*Li* - like ions. Finally, that denoted by R_f, calculated for almost flat in the core and peaked at the plasma edge, also related to R-equilibrium (with *He*/*Li* – like ions). The calculations shown in Figure 7(b) show that a change of the levels *He*/*Li* (in *R*-equilibrium) to *He*/*H* (in *S*-equilibrium) leads to a significant decrease in *D*. This is obviously due to the low ionization and recombination rates of *He*-like and *H*-like ions.

Figure 7 (c) shows the profiles $\xi_n = n_n / n_e$ that determine the rate profiles of recombination through charge-exchange of impurity ions on hydrogen neutrals and, hence, their corresponding equilibrium functions (26). Two regions of these equilibrium profiles for *S*-equilibrium (*He*/*H*) and for *R*-equilibrium (*He*/*Li*) are separated from each other by a narrow transition region depending on the plasma parameters that provide equilibrium. The gradual transition of impurity from *R*-equilibrium to *S*-equilibrium related to an increase in the average charge $< Z >= \sum_{k=0}^{Z} k \cdot f_k$.

This transition requires a noticeable decrease in the charge-exchange rates across the entire plasma cross-section, and especially at the periphery. Even small fluctuations in the plasma parameters (e.g., $\xi_n = n_n / n_e$) at the equilibrium boundary can cause a transition between the *S*- and *R*-equilibrium regions along with a significant change in the values of *D* and τ_p. But since this is a

Preprints (www.preprints.org) | NOT PEER-REVIEWED | Posted: 23 December 2020 doi:10.20944/preprints202012.0574.v1

transition from region (22) to (21), it can only occur in a jump. Figure 7 (d) shows how the corresponding changes in λ occurs when trying to gradually vary the parameters.

The modeling calculations of CS equilibrium of Ar were performed for a variety of $T_e(0)$, $T_i(0)$ and profiles $\xi_n(\rho)$ close to the modelled [17] conditions at JET [29, 30, 32]. Thus, the studied CS equilibrium of the types discussed above can be represented in a very wide range of these plasma parameters, revealing the corresponding range of λ and τ_p.

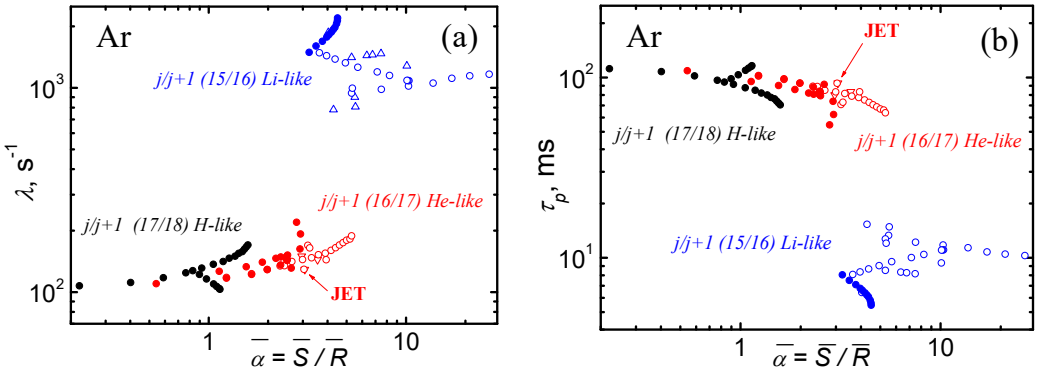

Figure 8. Model calculations of equilibrium constant (a) and confinement time (b) calculated for Ar by Formula (42) with *m*=12, various $j/j+1$ (as denoted), the equilibrium base (for *S*-equilibrium – full symbols and for *R*– equilibrium – open symbols), $T_e(0)$ and $T_i(0)$ varying within 1.5-8 keV, corresponding $\xi_n(\rho)$, $n_e = (4-9)\cdot 10^{19} m^{-3}$. The points denoted by JET correspond to the modelling data from JET [17].

Figures 8 summarizes these variations of equilibrium values λ (a) and τ_p (b) caused by the change in the temperatures $T_e(0)$ and $T_i(0)$ from 1.5 to 8 keV and by the corresponding (to equilibrium) variations of $\xi_n(\rho)$ (from the core to the equilibrium boundary) at an almost constant plasma density profile with $n_e(0) = 4.5\cdot 10^{19} m^{-3}$. Full symbols correspond to *S*- , and open symbols to *R*-equilibrium type. The growth of $T_e(0)$ leads to a noticeable increase in λ along with the increase $\bar{\alpha}(T_e)$. Increase $\xi_n(0)$ changes a lot $\bar{\alpha} \propto 1/\bar{R}[\xi_m(0)]$, but it does not change much $\lambda = \bar{S}(1+1/\bar{\alpha})$, since $\bar{\alpha} \approx 4$. An increase in $T_e(0)$ results in an increase $\bar{\alpha}(T_e, T_i) = \bar{S}(T_e)/\bar{R}(T_i)$, that is, to a shift of the obtained points on Figures 8 to the right. Figure 8 (b) shows the corresponding calculations of τ_p on Formula (42).

These estimations of τ_p generally correspond to the measurements and known τ_p scaling for L-, I- and H-modes [36, 37]. In particular, the estimates $\tau_p \approx 5-20$ ms for j/j+1 = 15/16 (Li- and He-like Ar) (see in Figure 8(b)) turns out to be in good agreement with scaling for L-mode plasmas [36] and for I-mode in Alcator C-Mode [37], but taking into account its higher plasma density $n_e(0) \approx 2\cdot 10^{20} m^{-3}$. Moreover, the calculated dependence $\tau_p(T_e)$ clearly shows the same tendency of slow decreasing with strongly increase in $T_e(0)$ from 1.5 up to 4 keV (see, e.g., Figure 4 in [37]). The transition from L- to H-mode plasmas results in a stepwise increase in $\tau_p \approx 50-1000$ ms [36-38] and corresponds to impurity equilibrium (both *S*- and *R*-type) for higher levels $j/j+1$= 16/17 (He- and H- like Ar) and $j/j+1$= 17/18 (H-like and full stripped Ar ions).

3.5. The radial scale of the CS equilibrium

As follows from Formulas (37) and (42), the radial number of equilibrium cells *m* plays a significant role in the scale factors of the impurity CS transport. The number of radial cells *m* was initially determined by the number of times on average the particle changes its CS moving from the

 doi:10.20944/preprints202012.0574.v1

center to the grid boundary. However, there is an inevitable contribution in m of the other transport processes. Therefore, it is not entirely clear how m is defined. Indeed, it could be assumed that collisional and/or turbulent transport in the plasma can contribute to m along with atomic processes, e.g., as a simple sum $m = m_{at} + m_{coll} + m_{turb}$. The simulations of the CS equilibrium transport show that it is necessary $m \approx 10$ for C, $m \approx 12-14$ for Ar and $m \approx 22-24$ for W. But for C, the largest excess over the reasonable estimates $m_{at} \approx 2-3$ (≤ 6 at least) is obtained, whereas for medium and heavy impurities, it can be assumed that $m_{coll} + m_{turb} \le 2-5$. It is worth noting that $\lambda \propto n_e$. But in accordance with Formula (42) $m \approx \lambda \tau_p$. So, if we assume that $m_{coll} \propto n_e$, then from $D \propto \lambda / (m+1)^3$, we can get a slowly decreasing dependence $D(n_e)$ as observed in experiments with light impurities (see, e.g., in [12, 40]).

Meanwhile, the simulation results are very weakly dependent on the value of m. For example, Figure 9 (a) shows calculations of the dependence $\lambda(m)$ for two types of equilibrium that differ in the total density profile (see Figure 7 (a)). So, λ is weakly sensitive to m, that is, to the radial dimensions of EC's over a wide range. Similarly, the value λ is weakly sensitive to $T_e(0)$, while maintaining the shape of the profile $T_e(\rho)$. It should be remembered that the ionization rates usually vary slowly near their maxima, depending on the temperature.

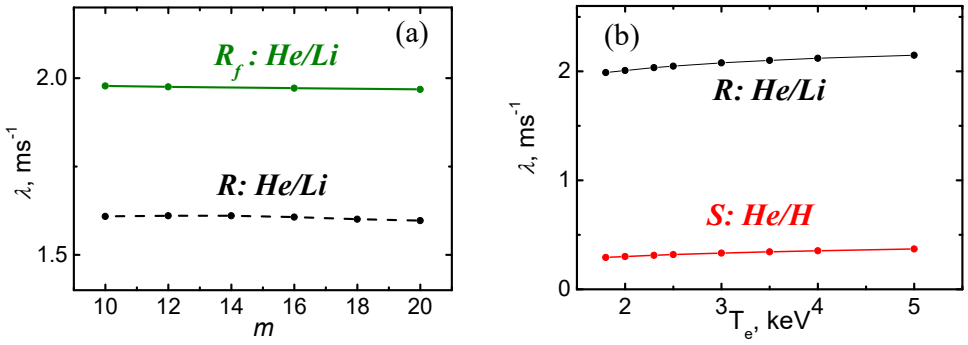

Figure 9. The equilibrium constant of Ar in dependence on (a) the number of cells m; (b) on the central plasma electron temperature $T_e(0)$.

4. The recovery of CS equilibrium on the density profile

As noted above, it is possible to change the formulation of the problem of equilibrium modelling to use the total density profile, $n_Z(\rho)$, usually known from experiments (or assumed to be given) with the data about ionization rates. Then, the recombination rates could be recovered along with the equilibrium transport rates. Such a formulation can be based on solving Equation (15) after reducing GM to a set of separate REC's. However, to solve it, it is necessary to have at least approximate data on λ as an input parameter, while the exact value is calculated as follows

$$\lambda = \sum_{n=1}^{m+1} \left(S_{jn} \varphi_{jn} + R_{j+1n} \varphi_{j+1n} \right), \tag{43}$$

where, initially, knowledge of the functions φ_{jn} and φ_{j+1n} is required. Nevertheless, the estimates show that using the total density profile $\{p_n\}$ (i.e. the profile $n_Z(\rho)$ taken form the experiment), the approximation $\lambda_{est} \approx \lambda$ can be found by the following formula

$$\lambda_{est} \approx \sum_{n=1}^{m+1} \left(S_{jn} + R_{j+1n} \right) \cdot p_n . \tag{44}$$

Preprints (www.preprints.org) | NOT PEER-REVIEWED | Posted: 23 December 2020 doi:10.20944/preprints202012.0574.v1

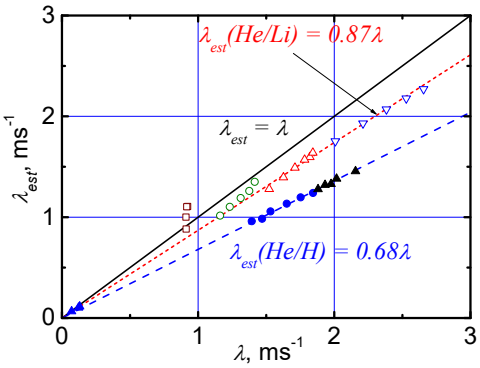

Figure 10. A comparison of the calculations using the exact Formula (43) and the approximate Formula (44) in the various equilibrium cases of C and Ar. Points shown with open symbols are related to *He*/*Li* equilibrium of Ar, while full symbols are of the *He*/*H* equilibrium type. Carbon data ($j/j+1$ are *H*-like ions and nucleous) are shown in black triangles.

Calculations of λ using Formulas (43) and (44) for C and Ar are compared in Figure 10. It is seen that all these data can be represented within a good accuracy by two approximate relations. For impurity equilibrium within the K-shell, choosing $j/j+1$ of *He*- and *H*-like ions, we get $\lambda_{est}(K) = 0.68 \cdot \lambda$ for both C and Ar, whereas within $j/j+1$ of *He*- and *Li*-like ions we obtain $\lambda_{est}(KL) = 0.87 \cdot \lambda$. So, a reasonable approximation $\lambda_{est} \approx \lambda$ to the exact equilibrium value depends on knowledges of (i) the basis of the equilibrium and (ii) the atomic structure of the most abundant impurity ions. Even rough estimates of the rates of ionization-recombination processes, normalized by an approximate value λ_{est}, provide the necessary input data for modelling using Formula (15) to reduce GM to REC.

Experiments with carbon pellet injection on the LHD stellarator [41] were chosen for modeling, since a large variety of carbon density profiles was observed there. The direct calculation of carbon equilibrium and its quasi-stationary temporal evolution was performed in [17]. These data turn out to be helpful when setting up the proposed recovery model of the profile $\xi_n(\rho)$. So, the recovery model directly uses as input data and reproduces exactly the profiles $n_C(\rho)$ observed in the LHD. The calculated profiles $\xi_n(\rho)$ (and the corresponding charge-exchange recombination rates) are found by an iterative procedure from the calculations of equilibrium. The convergence of iteration procedure in the recovery case is achieved in 8-10 iterations, which is noticeably faster compared to TICS, where it is achieved in only 30-40 iterations.

Figure 11 (a) shows the experimental profiles $n_C(\rho)$ adopted to discrete case, that is, $\{p_n\}$ at $t_1 = 1.83$ s, $t_2 = 2.03$ s, $t_3 = 2.23$ s, $t_4 = 2.54$ s, which are the input data of the model under consideration, except for the profile with carbon accumulation in the center, denoted by the letter A. As noted in [17], this A profile was modelled using data from the L-mode at $t_1 = 1.83$ s. Figure 11 (b) shows the diffusion coefficient profiles $D(\rho)$ calculated on Formula (37). Here we obtain the main feature of equilibrium CS transport in the plasma core, also found in experiments [25], in modelling [17] and revealed by the calculations of the profiles $\{\tilde{w}_n\}$ and $\{\tilde{u}_n\}$ presented above in Figure 5 (b): the lower the relative impurity density in the core, the higher $D(0)$. Conversely, the more impurity accumulates in the center, the smaller $D(0)$ required for such an equilibrium.

Preprints (www.preprints.org) | NOT PEER-REVIEWED | Posted: 23 December 2020 doi:10.20944/preprints202012.0574.v1

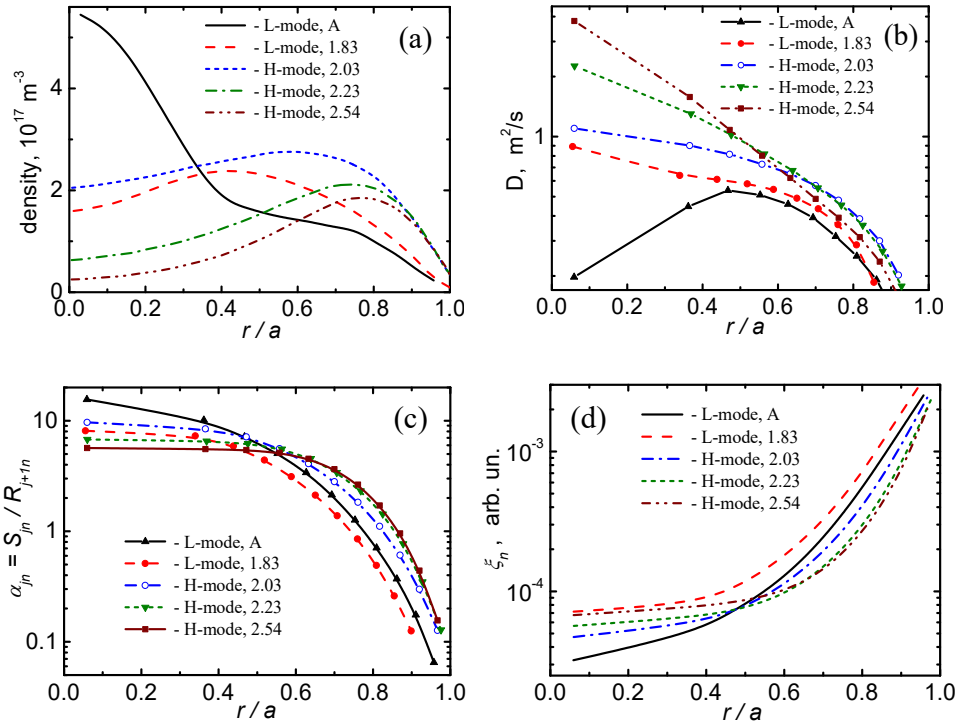

Figure 11. The calculated quasi-stationary equilibrium of C in L-mode at $t_1 = 1.83$ s^{-1} along with modelled central accumulation (curves A) and in H-mode at $t_2 = 2.03$ s^{-1}, $t_3 = 2.23$ s^{-1}, $t_4 = 2.54$ s^{-1}: (a) input total density profiles measured in the experiment [41]; (b) the profiles of diffusion coefficient, calculated according to Formula (37); (c) the equilibrium functions; (d) calculated profiles of the relative density of hydrogen neutrals.

Figure 11 (c) shows the calculation of the quasi-stationary temporal evolution of the equilibrium function, its successive noticeable flattening and displacement of the sharp edge to the periphery of the plasma column along with the maximum of the density profile $n_C(\rho)$. The resulting profiles $\xi_n(\rho)$ also change sequentially showing a flattening in the plasma core and a decrease in the density of neutrals at the plasma periphery, where the maximum of $n_C(\rho)$ shifts. It should be noted that, in general, the obtained novel results are in reasonable agreement with the data of direct modeling of the equilibrium CS transport by the TICS code [17].

5. Conclusions

The impurity CS transport is a typical transport process in plasma, which finds its place in a range of other transport processes. This fundamentally 2D transport is consistently represented by symmetric differential and discrete forms of FPKE. The concept of impurity CS equilibrium transport provides an understanding of the crucial role of atomic processes in the behavior of plasma impurities. The impurity equilibrium observed in experiments together with a large variety of impurity density profiles, both total and partial, in a stationary plasma is essentially a double coronal equilibrium (DCE). DCE is a direct consequence of the symmetric properties of the discrete FPKE (7) and of the conservation law of CS's moving in the proper phase space.

Nonlinear problems of analysis of 2D CS equilibrium and transport are significantly simplified by reducing the original GM to a whole set of simple schemes (see Figure 4) using the pseudo-state technique together with reduction invariants. The most important of them is the equilibrium constant, λ, which determines the general time scale of the impurity equilibrium in a stationary plasma. It provides crucial information to understand the scale of equilibrium transport rates and confinement time of impurities in hot plasmas.

In particular, the difference of the behavior and transport of impurities in plasma is determined by their ionization-recombination rates values that is, by the dependence $\lambda(Z)$, analysis of which is the immediate task. Naturally, the impurity equilibrium and transport in hot plasma depend on the atomic structure of impurity ions that define the equilibrium levels for the most abundant ions as discussed above.

A significant difference of 3-10 times both in the values of *D* (see Fig. 7 (b)) and in the values τ_p (see Figures 7 and 8) in various types of CS equilibrium suggests their direct coupling with the observations of impurities in the L-, I -, and H-modes in plasma [24, 37]. The estimates τ_p made on the basis of CS transport modelling of C and Ar are in good agreement with the known experimental scaling [36] and measurements [37].

The coupling of the profile $\{p_n\}$ with the rates of particle transport makes it possible to directly analyze typical profiles $\tilde{D}(\rho)$ and $\tilde{v}(\rho)$ observed in experiments, in particular, for the central accumulation or any other distribution of impurities in the plasma cross-section. It is shown that using REC analysis, data on $\{p_n\}$, ionization-recombination rates and the proposed approximation of λ (see Formula (44)), it is also possible to solve the recovery problem for rate profiles along with equilibrium CS transport analysis. In particular, it is possible to calculate the relative profile of neutral hydrogen, which determines the charge-exchange recombination rate of light and medium impurities.

Thus, the concept of impurity CS transport opens up significant prospects for direct analysis of the rates of ionization-recombination processes in a hot quasi-stationary plasma.

Acknowledgments: Author would like to thank Prof. Dr. V. S. Lisitsa and Dr. E. I. Yurchenko for helpful discussions and valuable notes. Author is grateful to Dr. V. E. Zhogolev for providing useful software in calculating ionization and recombination rates.

References

1. Köchl F., Loarte A., de la Luna E., Parail V., Corrigan G., Harting D., Nunes I., Reux C., Rimini F. G., Polevoi A., Romanelli M. and JET Contributors. W transport and accumulation control in the termination phase of JET H-mode discharges and implications for ITER. *Plasma Phys. Control. Fusion.* 2018, 60, 074008(21pp). [https://doi.org/10.1088/1361-6587/aabf52]
2. Mukai K., Nagaoka K., Takahashi H., Yokoyama M., Murakami S., Nakano H., Ida K., Yoshinuma M., Seki R., Kamio S., Fujiwara Y., Oishi T., Goto M., Morita S., Morisaki T., Osakabe M. and the LHD Experiment Group. Carbon impurities behavior and its impact on ion thermal confinement in high-iontemperature deuterium discharges on the Large Helical Device. *Plasma Phys. Control. Fusion.* 2018, 60, 074005(7pp). [https://doi.org/10.1088/1361-6587/aac06c]
3. Kolmogoroff A. N. Über die analytischen Methoden in der Wahrscheinlichkeitsrechnung. *Math. Ann.* 1931, 104, 415-458. [https://doi.org/10.1007/BF01457949]
4. Kolmogoroff A. Zur Theorie der stetigen zufälligen Prozesse. *Math. Ann.* 1933, 108, 149-160. [https://doi.org/10.1007/BF01452829]
5. Caughey T. K. Derivation and application of the Fokker-Plank Equation to discrete nonlinear dynamic systems subjected to white random excitation. *Journal of the Acoustical Society of America* 1963, 35, 1683-1692. [https://doi.org/10.1121/1.1918788]
6. Dux R. *STRAHL User Manual Technical Report*. IPP 10/ 30 IPP Max-Planck-Istitut für Plasmaphysik. 2006. Available online: content (mpg.de)
7. Bertschinger G et al 1999 Proc. 26th EPS Conf. on Controlled Fusion Plasma Physics ECA vol 23J (Maastricht, 14 -18 June 1999) P2.018, p 661. Available online: http://epsppd.epfl.ch/Maas/web/pdf/p2018.pdf
8. Sertoli M., Angioni C., Dux R., Neu R., Pütterich T., Igochine V. and the ASDEX Upgrade Team. Local effects of ECRH on argon transport in L-mode discharges at ASDEX Upgrade. *Plasma Phys. Control. Fusion*. 2011, 53, 035024 (21pp). [https://doi.org/10.1088/0741-3335/53/3/035024]

9. Stratton B.C., Ramsey A.T., Boody F.P., Bush C.E., Fonck R.J., Groebner R.J., Hulse R.A., Richards R.K., Schivell J. Spectroscopic study of impurity behaviour in neutral beam heated and ohmically heated TFTR discharges. *Nucl. Fusion*. 1987, 27, 1147-1164. [https://doi.org/10.1088/0029-5515/27/7/008]
10. Demokan O., Waelbroeck F., Demokan N. Iron transport in a confined high-temperature plasma. *Nucl. Fusion*. 1982, 22, 921-934. [https://doi.org/10.1088/0029-5515/22/7/005]
11. Content D.A., Moos H.W., Perry M.E., Brooks N.H., Ali Mahdavi M., Petrie T.W., John H. St., Schisse D.P., Hulse R.A. Impurity profiles for H-mode discharges in DIII-D. *Nucl. Fusion*. 1990, 30, 701-716. [https://doi.org/10.1088/0029-5515/30/4/011]
12. Stratton B.C., Fonck R.J., Hulse R.A., Ramsey A.T., Timberlake J., Efthimion P.C., Fredrickson E.D., Grek B., Hill K.W., Johnson D.W., Mansfield D.K., Park H., Stauffer F.J., Taylor G. Impurity transport in ohmically heated TFTR plasmas. 1989, 29, 437-448 [https://doi.org/10.1088/0029-5515/29/3/007]
13. Suckewer S., Cavallo A., Cohen S., Daughney C., Denne B., Hinnov E., Hosea J., Hulse R., Hwang D., Schilling G., Stratton B., Wilson R. Impurity ion transport studies on the PLT tokamak during neutral-beam injection. *Nucl. Fusion*. 1984, 24, 815-826. [https://doi.org/10.1088/0029-5515/24/7/001]
14. Asmussen K., Fournier K.B., Laming J.M., Neu R., Seely J.F., Dux R., Engelhardt W., Fuchs J.C. and ASDEX Upgrade Team. Spectroscopic investigations of tungsten in the EUV region and the determination of its concentrations in tokamaks. *Nucl. Fusion*. 1998, 38, 967-986. [https://doi.org/10.1088/0029-5515/38/7/302]
15. Pütterich T., Neu R., Dux R, Whiteford A. D., O'Mullane M.G. and the ASDEX Upgrade Team. Modelling of measured tungsten spectra from ASDEX Upgrade and predictions for ITER. *Plasma Phys. Control. Fusion* 2008, 50, 085016 (27pp) [https://doi.org/10.1088/0741-3335/50/8/085016]
16. Hirshman S.P., Sigmar D.J. Neoclassical transport of impurities in tokamak plasmas. *Nucl. Fusion*. 1981, 21, 1079-1202. [https://doi.org/10.1088/0029-5515/21/9/003]
17. Shurygin V.A. Impurity charge state transport in tokamak and stellarator plasmas. *Nucl. Fusion.* 2020, 60, 046001 (18pp) [https://doi.org/10.1088/1741-4326/ab6871]
18. Shurygin V.A. Anomalous impurity transport: charge-state diffusion due to atomic processes in tokamak plasmas. *Plasma Phys. Control. Fusion*. 1999, 41, 355-375. [https://doi.org/10.1088/0741-3335/41/3/003]
19. Shurygin V.A. Kinetics of impurity charge-state distributions in tokamak plasmas. *Plasma Phys. Rep.* 2004, 30, 443–472. [https://doi.org/10.1134/1.1768581]
20. Shurygin V.A. Analytical approach to impurity transport studies: Charge state dynamics in tokamak plasmas. *Phys. Plasmas.* 2006, 13 082506 (14pp) [https://doi.org/10.1063/1.2335413]
21. Shurygin V.A. Analytical impurity transport model: Coupling between particle and charge state transports in tokamak plasmas. *Phys. Plasmas.* 2008, 15, 012506 () [https://doi.org/10.1063/1.2833589]
22. TFR Group. Space-resolved vacuum ultra-violet spectroscopy on T.F.R. Tokamak plasmas. *Plasma Physics*. 1978, 20, 207-223. [https://doi.org/10.1088/0032-1028/20/3/005]
23. TFR Group. Are heavy impurities in TFR Tokamak plasmas at ionization equilibrium? *Plasma Physics.* 1980, 22,851-860. [https://doi.org/10.1088/0032-1028/22/8/008]
24. Giannella R., Lauro-Taroni L., Mattioli M., Alper B., Denne-Hinnov B., Magyar G., O'Rourke J., Pasini D. Role of current profile in impurity transport in JET L mode discharges, *Nucl. Fusion*. 1994, 34, 1185-1202. [https://doi.org/10.1088/0029-5515/34/9/I01]
25. Dux R. Neu R., Peeters A.G., Pereverzev G., Mück A., Ryter F., Stober J. and ASDEX Upgrade Team. Influence of the heating profile on impurity transport in ASDEX Upgrade. *Plasma Phys. Control. Fusion.* 2003, 45, 1815-1826. [https://doi.org/10.1088/0741-3335/45/9/317]
26. Braginskii, S.I. 1965. Transport Processes in Plasma. *Reviews of Plasma Physics* ed M. A. Leontovich (New York: Consultants Bureau), 1, 205-311.
27. Wade M.R., Houlberg W.A., Baylor L.R., West W.P., Baker D.R. Low-Z impurity transport in DIII-D – observations and implications. *J. Nucl. Mater.* 2001, 290-293, 773-777. [https://doi.org/10.1016/S0022-3115(00)00499-2]
28. Kubo H., Sakurai S., Higashijima S., Takenaga H., Itami K., Konoshima S., Nakano T., Koide Y., Asakura N., Shimizu K., Fujita T., Hill K.W. Radiation enhancement and impurity behavior in JT-60U reversed shear discharges. *J. Nucl. Mater.* 2003, 313–316, 1197–1201. [https://doi.org/10.1016/S0022-3115(02)01531-3]
29. Puiatti M.E., Mattioli M., Telesca G., Valisa M., Coffey I., Dumortier P., Giroud C., Ingesson L.C., Lawson K.D., Maddison G., Messiaen A.M., Monier-Garbet P., Murari A., Nave M.F.F., Ongena J., Rapp J., Strachan J., Unterberg B., von Hellermann M. and contributors to the EFDA-JET Workprogramme. Radiation

pattern and impurity transport in argon seeded ELMy H-mode discharges in JET. *Plasma Phys. Control. Fusion*. 2002, 44, 1863–1878. [https://doi.org/10.1088/0741-3335/44/9/305]

30. Puiatti M.E., Valisa M., Mattioli M., Bolzonella T., Bortolon A., Coffey I., Dux R., von Hellermann M., Monier-Garbet P., Nave M.F.F., Ongena J. and contributors to the EFDA-JET Workprogramme. Simulation of the time behaviour of impurities in JET Ar-seeded discharges and its relation with sawtoothing and RF heating. *Plasma Phys. Control. Fusion*. 2002, 45, 2011-2024. [https://doi.org/10.1088/0741-3335/44/9/305]
31. Krupin V.A., Nurgaliev M.R., Klyuchnikov L.A., Nemets A.R., Zemtsov I.A., Dnestrovskij A.Yu., Sarychev D.V., Lisitsa V.S., Shurygin V.A., Leontiev D.S., Borschegovskij A.A., Grashin S.A., Ryjakov D.V., Sergeev D.S., Mustafin N.A., Trukhin V.M., Solomatin R.Yu., Tugarinov S.N., Naumenko N.N. Experimental study of tungsten transport properties in T-10 plasma. *Nucl. Fusion*. 2017, 57, 066041 (9pp) [https://doi.org/10.1088/1741-4326/aa69c5]
32. Mattioli M., Puiatti M.E., Valisa M., Coffey I., Dux R., Monier-Garbet P., Nave M.F.F., Ongena J., Stamp M., Strachan J., von Hellermann M. and contributors to the EFDA-JET Workprogramme. Simulation of the time behavior of impurities in Jet Ar-seeded discharges and its relation with sawteething. 2002. *29th EPS Conference on Plasma Phys. and Contr. Fusion.* (Montreux, 17-21 June) ECA Vol. 26B (Geneva: EPS) P2.042 (CD-ROM). Available online: http://epsppd.epfl.ch/Montreux/pdf/P2_042.pdf
33. Segiun F.H., Petrasso R., Marmar E.S. Effects of Internal Disruptions on Impurity Transport in Tokamak. *Phys. Rev. Let*. 1983, 51, 455-458. [https://doi.org/10.1103/PhysRevLett.51.455]
34. Leung W.K., Rowan W.L., Wiley J.C., Braveneck R.V., Gentle K.W., Hodge W.L., Patterson D.M., Phillips P.E., Price S.R., Richards B. Interpretation of impurity confinement time measurements in tokamaks. *Plasma Phys. Control. Fusion*. 1986, 28, 1753-1764. [https://doi.org/10.1088/0741-3335/28/12A/002]
35. Fussmann G. Analytical modelling of impurity transport in toroidal devices. *Nucl. Fusion* 1986, 26, 983-1002. [https://doi.org/10.1088/0029-5515/26/8/001]
36. Mattioli M., Giannella R., Myrnas R., Demichelis C., Denne-Hinnov B., Dudok De Wit T., Magyar G. Laser blow-off injected impurity particle confinement times in JET and Tore Supra. *Nucl. Fusion.* 1995, 35, 1115-1124. [https://doi.org/10.1088/0029-5515/35/9/I05]
37. Rice J.E., Reinke M.L., Gao C., Howard N.T., Chilenski M.A., Delgado-Aparicio L., Granetz R.S., Greenwald M.J., Hubbard A.E., Hughes J.W., Irby J.H., Lin Y., Marmar E.S., Mumgaard R.T., Scott S.D., Terry J.L., Walk J.R., White A.E., Whyte D.G., Wolfe S.M., Wukitch S.J. Core impurity transport in Alcator C-Mod L-, I- and H-mode plasmas. *Nucl. Fusion.* 2015, 55, 033014 (12pp). [https://doi.org/10.1088/0029-5515/55/3/033014]
38. Perry M.E., Brooks N.H., Content D.A., Hulse R.A., Ali Mahdavi M., Moos H.W. Impurity transport during the H-mode in DIII-D. *Nucl. Fusion*. 1991, 31, 1859-1876. [https://doi.org/10.1088/0029-5515/31/10/005]
39. Pasini D., Giannella R., Taroni L.L., Mattioli M., Denne-Hinnov B., Hawkes N., Magyar G., Weisen H. Measurements of impurity transport in JET. *Plasma Phys. Control. Fusion.* 1992. 34, 677-686. [https://doi.org/10.1088/0741-3335/34/5/002]
40. Krieger K., Fussmann G., and the ASDEX Team. Determination of impurity transport coefficients by harmonic analysis. *Nucl. Fusion*. 1990, 30, 2392-2396. [https://doi.org/10.1088/0029-5515/30/11/015]
41. Ida K.,_ Yoshinuma M., Osakabe M., Nagaoka K., Yokoyama M., Funaba H., Suzuki C., Ido T., Shimizu A., Murakami I., Tamura N., Kasahara H., Takeiri Y., Ikeda K., Tsumori K., Kaneko O., Morita S., Goto M., Tanaka K., Narihara K., Minami T., Yamada I. and LHD Experimental Group. Observation of an impurity hole in a plasma with an ion internal transport barrier in the Large Helical Device. *Phys. Plasmas.* 2009, 16, 056111 (9pp). [https://doi.org/10.1063/1.3111097]